Check for updates

RESEARCH ARTICLE

Extruded Tunnel Lining Regeneration Project (ETLR): experimental campaign on real scale SFRC tunnel mock-ups

[version 1; peer review: awaiting peer review]

Andrea Marcucci[1], Stefano Guanziroli[2], Marco Borroni[2], Bernardino Chiaia[3], Liberato Ferrara[1], Marco Peroni[4], Marco Lamperti Tornaghi[4], Francisco Javier Molina[4], Simone Peloso[4], Daniel A. Pohoryles[4], Georgios Tsionis[4]

[1]Department of Civil and Environmental Engineering, Politecnico di Milano, Milan, Lombardy, 20133, Italy
[2]Hinfra s.r.l., Casale Monferrato, Italy
[3]Politecnico di Torino Department of Structural, Building and Geotechnical Engineering, Torino, Piemonte, Italy
[4]European Commission Joint Research Centre Ispra, Ispra, Lombardy, Italy

v1 **First published:** 22 Sep 2026, **6**:371
https://doi.org/10.12688/openreseurope.23554.1
Latest published: 22 Sep 2026, **6**:371
https://doi.org/10.12688/openreseurope.23554.1

Abstract

Background

Automation in the construction industry is gaining increasing relevance, driven by the need to enhance productivity, foster innovation, and meet evolving societal demands. Slip-forming with extrudable steel fibre-reinforced concrete (SFRC) offers an innovative framework for the maintenance and refurbishment of highway and railway tunnels. However, its structural performance requires full-scale validation before adoption in practice.

Methods

Four full-scale mock-ups replicating a motorway tunnel lining were constructed using slip-forming with extrudable SFRC and tested under load conditions simulating the relevant action combinations for tunnel linings in the intended scenarios. Both symmetric and non-symmetric loading combinations were examined, including a sequential loading case to assess accumulated damage and residual bearing capacity. Digital Image Correlation (DIC) analysis was performed to study cracking in the mock-ups, enabling computation of crack opening, which was related to the load applied by the hydraulic jacks employed in the experiment. Testing was conducted at the ELSA laboratory of the European Commission, Joint Research Centre in Ispra, as part of

Open Peer Review

Approval Status *AWAITING PEER REVIEW*

Any reports and responses or comments on the article can be found at the end of the article.

the OPENLAB ETLR project.

Results

The relationship between crack opening and applied load enabled characterisation of the post-cracking residual capacity of the SFRC tunnel lining structure under the tested loading combinations, including its behaviour under sequential loading and the associated accumulation of damage.

Conclusions

The full-scale tests provide a preliminary validation of the adopted design criteria and an assessment of the effectiveness and structural reliability of the proposed slip-forming SFRC technology for tunnel lining refurbishment.

Keywords
Tunnel, Slip-forming, Maintenance, SFRC

This article is included in the Joint Research Centre gateway.

Corresponding author: Stefano Guanziroli (stefano.guanziroli@hinfra.it)

Author roles: Marcucci A: Formal Analysis, Software, Writing – Original Draft Preparation; **Guanziroli S**: Conceptualization, Methodology, Project Administration, Supervision, Writing – Original Draft Preparation; **Borroni M**: Conceptualization, Project Administration, Supervision; **Chiaia B**: Conceptualization; **Ferrara L**: Conceptualization, Supervision, Writing – Review & Editing; **Peroni M**: Conceptualization, Data Curation, Software; **Lamperti Tornaghi M**: Conceptualization, Supervision; **Molina FJ**: Conceptualization, Data Curation; **Peloso S**: Data Curation, Writing – Review & Editing; **Pohoryles DA**: Data Curation, Writing – Review & Editing; **Tsionis G**: Data Curation, Writing – Review & Editing

Competing interests: The second and third authors are employees of Hinfra s.r.l, which is a partner of the project and funded the specimens. Hinfra s.r.l. commercialises the Extruded Tunnel Lining Regeneration train able to complete the regeneration of existing tunnels in an automatic manner

Grant information: This project has received funding from the Joint Research Centre Physical Research Infrastructures of the European Commission under Research Infrastructure Access Agreement No 36506-1 / 2021-1-RD-ELSA-ReactionWall (ETLR project). This research was generated through access to the ELSA Reaction Wall.
The funders had no role in study design, data collection and analysis, decision to publish, or preparation of the manuscript.

Copyright: © 2026 Marcucci A *et al*. This is an open access article distributed under the terms of the Creative Commons Attribution License, which permits unrestricted use, distribution, and reproduction in any medium, provided the original work is properly cited.

How to cite this article: Marcucci A, Guanziroli S, Borroni M *et al.* **Extruded Tunnel Lining Regeneration Project (ETLR): experimental campaign on real scale SFRC tunnel mock-ups [version 1; peer review: awaiting peer review]** Open Research Europe 2026, **6**:371 https://doi.org/10.12688/openreseurope.23554.1

First published: 22 Sep 2026, **6**:371 https://doi.org/10.12688/openreseurope.23554.1

Introduction

Tunnels are the most strategic type of infrastructure. Their construction has been pivotal for the development of the modern society. In fact, tunnels are indispensable in connecting areas separated by mountains, rivers or urban congestion, often working as critical arteries in transportation and utility systems. The construction of new tunnels for the infrastructural development has been substantial, especially starting from the last century.[1] Nowadays, the construction of new tunnels (especially related to transportation needs) is still highly relevant, and new excavation techniques have been introduced in addition to the traditional drill and blast method,[2,3] as for example the Tunnel Boring Machine (TBM).[4] This new technology permits a faster tunnel excavation and lining construction, depending on the environmental conditions, as well as the geometry of the tunnel to be built.[5,6]

However, in parallel to the construction of new tunnels, maintenance plays a critical role in guaranteeing the structural integrity of damaged existing tunnels. The start-up company Hinfra has decided to move towards this direction, introducing a new methodology for the complete refurbishment of existing tunnels.[7] As reported in Figure 1, the company has developed a train composed of different modules, able to complete the regeneration of existing tunnels in an automatic manner. The heading module of the train is characterised by scraping devices with the aim of removing the deteriorated layer of the old tunnel. Other modules follow the first one, which are responsible for the movement of the train. Finally, a last module works as formwork for the casting of the new tunnel lining. After the completion of the casting of a lining segment, based on the concrete strength development, the train advances extruding segments of the new tunnel lining. From the material point of view, the new concrete lining applied to the existing tunnel consists of steel fibre reinforced concrete (SFRC). This type of advanced material is characterised by a non-negligible tensile strength compared to plain concrete, thanks to the fibre bridging effect.[8,9] Fibres are efficient in working as bridges between two cracked concrete surfaces, conferring a post-cracking strength to the material. Their main failure mechanism is the pull-out,[10,11] which provides toughness to concrete. The effect of the fibre reinforcement can be observed experimentally on small samples. In particular, direct or indirect tensile tests are generally performed to evaluate the toughness of SFRC mixes.[12,13] The most diffused type of test is the three-point bending test, which consists of a flexural test able to provide a Mode I fracture on the mid-span cross-section of the sample. Model Code 2010 has introduced a procedure based on the three-point bending test to compute the uniaxial tensile constitutive law for SFRC.[14,15] The experimental results for the characterisation of the material behaviour of SFRC are influenced by a large dispersion due to the random distribution of the fibres. Depending on the distribution of the fibres, the behaviour of a specific cross-section may differ.[16] Especially the fibre orientation with respect to the normal direction of the cracked cross-section is a parameter governing the post-cracking strength of SFRC mixes.

As reported by the authors in,[17,18] depending on the orientation of fibres affected by the casting procedure, the structural behaviour of SFRC beams becomes completely different. Predicting the orientation of fibres in the concrete matrix is crucial for a proper evaluation of the mechanical properties.[19] Fibres tend to follow the flow paths forming during casting of fluid concrete. The well-known "wall-effect" provided by the boundaries of the formwork during casting of concrete is fundamental in influencing the fibre orientation.[20] However, the fibre distribution and orientation can also be predicted by numerical methods.[21,22,23] These methods consist of the use of Computational Fluid Dynamics (CFD) tools, adopted for the simulation of concrete casting. However, the fibre distribution can also be assessed after the completion of casting, as quality control procedure, through non-destructive methods. A powerful methodology to monitor the fibre distribution in a medium is through the use of a magnetic device, introduced by.[24,25] According to this magnetic method, it is possible to check the fibre distribution in concrete simply leaning the sensor on the element surface.

If the fibre contribution on the post-cracking strength of concrete is evident, the fibres can be adopted for structural uses without the need of ordinary steel reinforcement. From a practical point of view, the solution of a full fibre reinforced concrete element is more convenient, as it does not need the placement of steel rebars. This is evident on tunnel applications, where the placement of steel rebars is one of the most challenging steps. The choice of using only the fibre reinforcement is strategic for the introduced maintenance intervention, as the refurbishment can be completed in a fully automatic way, without the need of interruptions for the placement of steel reinforcements. Hence, the new SFRC lining applied on the damaged existing tunnel has a structural bearing function. In particular, the new lining is designed to work separately from the existing tunnel, which continues to provide the resistance to the external loading. However, when collapse of the existing tunnel occurs, the new lining is responsible for the structural integrity of the tunnel.

With the aim of validating the structural performance of the new tunnel lining, structural tests have been performed at the ELSA Reaction Wall of the European Commission, Joint Research Centre. Four identical tunnel segment mock-ups have been tested in this experimental campaign, in order to understand the load bearing capacity of the lining under different load combinations.

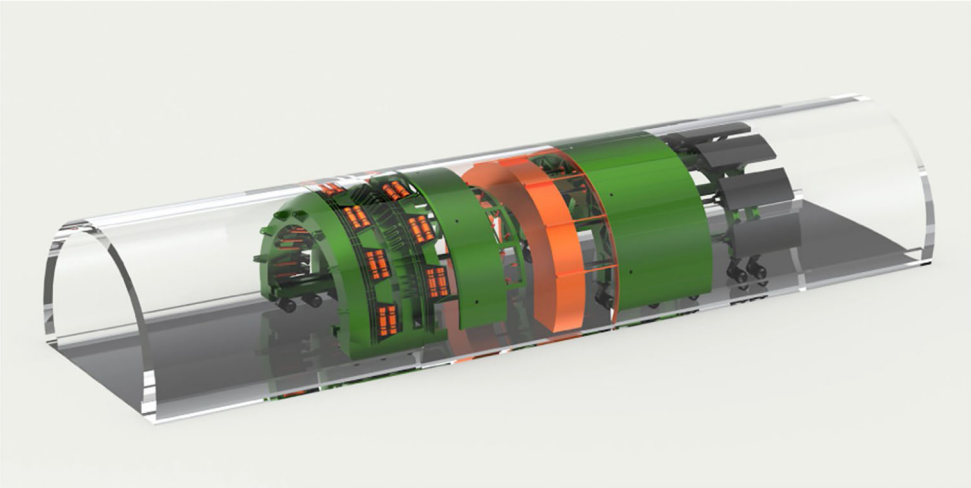


Figure 1. **The Extruded Tunnel Lining Regeneration train developed by Hinfra.**

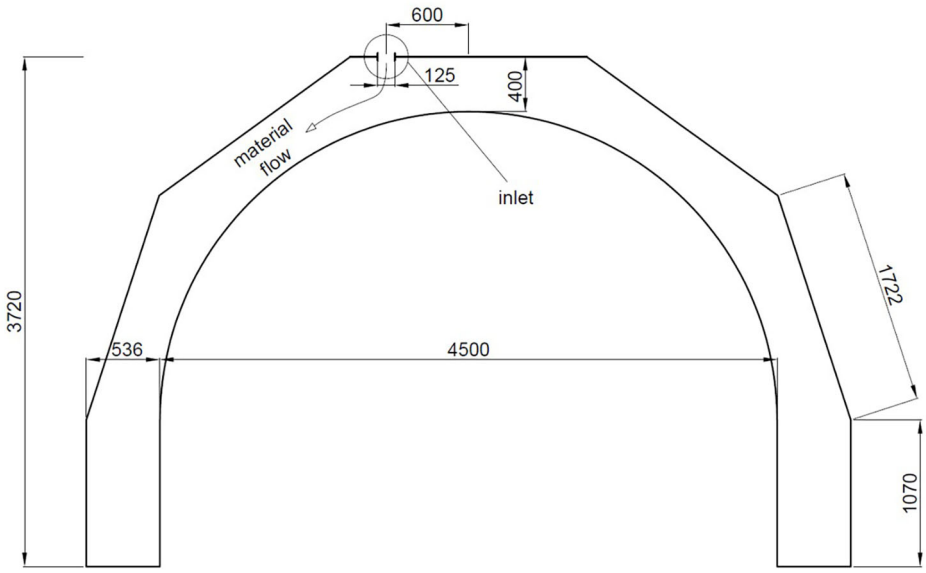


Figure 2. **Geometry of the tunnel mock-ups (dimensions in [mm]).**

Methods

Test specimens

The experimental campaign consists of four identical mock-ups (labelled SEGMENT00 to SEGMENT03) having the shape and dimensions of a one-lane tunnel. The geometry of the samples is reported in Figure 2. The height of the mock-up is almost four metres and its width is approximately five metres and a half. The thickness instead is variable along the hoop direction, with a maximum of half a metre in the bottom part of the mock-up.

The construction phases of the mock-ups are also evidenced in Figure 2. The specimens have been filled from the top region, in a position slightly at the left of the key in a hole of 125 mm. After the setting of concrete, the formwork was moved, sliding against the specimen, similarly to an extrusion, consisting of a manufacturing process that reflects the real ETLR application.

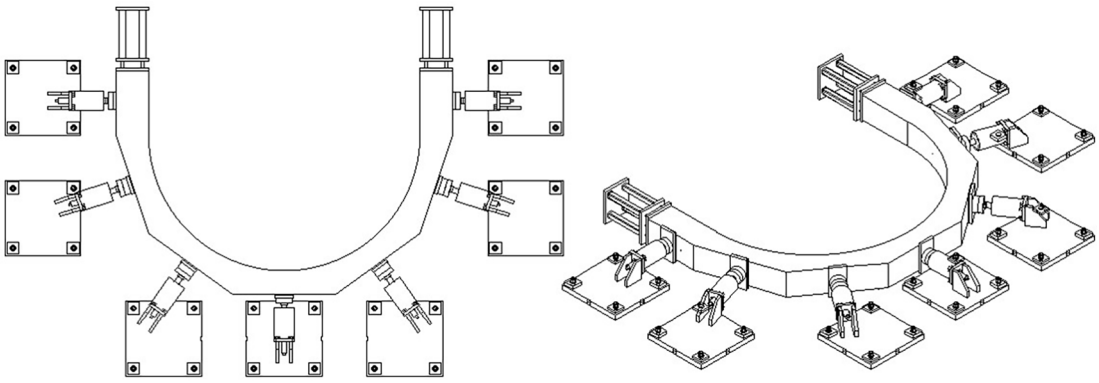
The material adopted in the manufacturing of the mock-ups is a SFRC, characterised by 0.5% of 3D Dramix fibres (volume percentage) of 60 mm length and 0.9 mm diameter. The concrete compressive strength is around 50 MPa,

whereas the tensile properties have been characterised from testing 12 identical beams under three-point bending load configuration, following EN 14651 procedure.[26] Based on the average values of the flexural residual strengths corresponding to a crack opening of 0.5 and 2.5 mm (namely f_{R1} and f_{R3}),a SFRC class of 10d is obtained according to Model Code 2010,[14] remarking the deflection hardening property of the composite.

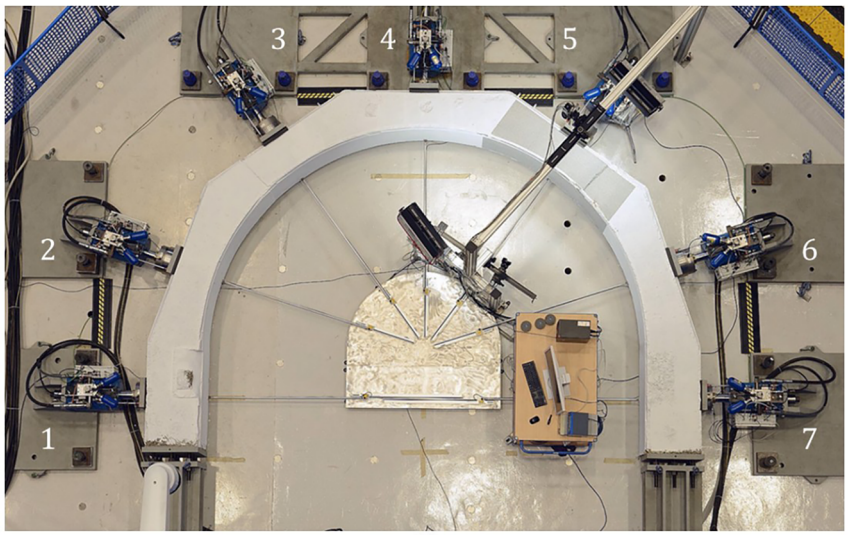
Set-up and instrumentation

The set-up designed for the experimental campaign is reported in Figure 3. The tunnel mock-up is simply supported on the ground and it is in contact with two steel column supports, which are connected to the Reaction Wall. Along the extrados surface seven actuators are placed at the midpoint of each side of the extrados perimeter of the mock-up, having a double function of loading or restraining the mock-up. The actuators have a capacity of 1 MN and total stroke of 450 mm. The loads were measured by load cells built-in the actuators. Each actuator is in contact with the mock-up through a steel plate, which redistribute the load applied. A second rubber layer is placed between the steel plate and the mock-up in order to assure a better contact between the parts. Additionally, as evident in Figure 3b, along the intrados surface seven displacement sensors (linear encoders) are placed in correspondence of each actuator. The calibration reports of force and displacement sensors are included in the dataset. For additional details about the interpretation of the calibration reports, the reader can refer to the Technical Report No JRC139347.[30]

Finally, a camera is positioned on top of the region corresponding to actuator 5 (see Figure 3b). The images of the latter were used for Digital Image Correlation (DIC) analysis in order to compute the displacement and strain fields; hence, a speckle pattern has been applied in the region of interest.



(a)



(b)

Figure 3. Set-up and instrumentation for the tunnel mock-ups.

Test programme

The tests performed in the experimental campaign followed a specific programme. In particular, preliminary tests were applied to the mock-up with the aim of assessing the stiffness of the specimen for different loading cases. Additionally, the mock-ups have been brought up to failure following two different loading combinations, LC1 and LC2 respectively. The first loading combination is non-symmetric, whereas the second one is symmetric. In Table 1 the different load cases for the preliminary tests are resumed along with the loading combinations adopted for tests up to collapse of the specimen. The numeration of the actuators is referred to the one reported in Figure 3b. Having the actuators a double function of loading or restraining the sample, a "0" is assigned in the table to the actuators working as restraint, and a "1" in case the actuators are loading the mock-up. Otherwise, the actuators are not working during the test.

All the tests have been conducted under displacement control, at a constant rate of the loading actuator of 0.6 mm/min. The first two mock-ups have been tested until failure following LC1, whereas the last two mock-ups following LC2. Moreover, the preliminary tests have been performed only for the second and third mock-up of the entire experimental campaign. The following Table 2 reports the lists of the experiments, including information on the segment tested.

Results

Preliminary load cases

Before the structural test up to failure of the mock-up, preliminary tests were performed in order to check the stiffness of the specimen under different load cases (the one reported in Table 1 in Roman numbers). The results are reported in Figure 4 in terms of load-displacement curves (load of the actuator and displacement of the sensor corresponding to the loading actuator), here reported only for SEGMENT01 and SEGMENT02.

It is worth noting that the curves for the two different mock-ups are similar for each load case. Varying the position of the load, from the bottom to the key of the mock-up the stiffness increases, resulting in a curve with a higher inclination. When the load is applied to the key, the arch effect of the mock-up is more evident, as the structure works mainly under compressive stresses. Instead, for lateral loading applied to the mock-up, the structure undergoes higher tensile stresses induced by the bending moments. Computing the stiffness as the initial inclination of the load-displacement curve, it is possible to compare the values obtained for the different load cases (Figure 4f). The variation of the stiffness highlights what has been discussed, obtaining for load case III a value of the stiffness double that of load cases I and V, also remarking the symmetric behaviour of the specimens.

Table 1. Loading cases for the preliminary tests and load combinations for the tests up to collapse of the mock-up.

Actuator							
Load case	**1**	**2**	**3**	**4**	**5**	**6**	**7**
I	-	1	-	-	-	-	0
II	-	-	1	-	-	-	0
III	0	-	-	1	-	-	0
IV	0	-	-	-	1	-	-
V	0	-	-	-	-	1	-
LC1	-	1	-	-	0	-	0
LC2	0	-	1	-	1	-	0

Table 2. Testing programme.

Experiment Tag	Specimen	Date	Load case
b02	SEGMENT00	19/06/2023	LC1
c02	SEGMENT01	25/07/2023	LC1
d02	SEGMENT02	01/12/2023	LC2
e02	SEGMENT03	12/03/2024	LC2

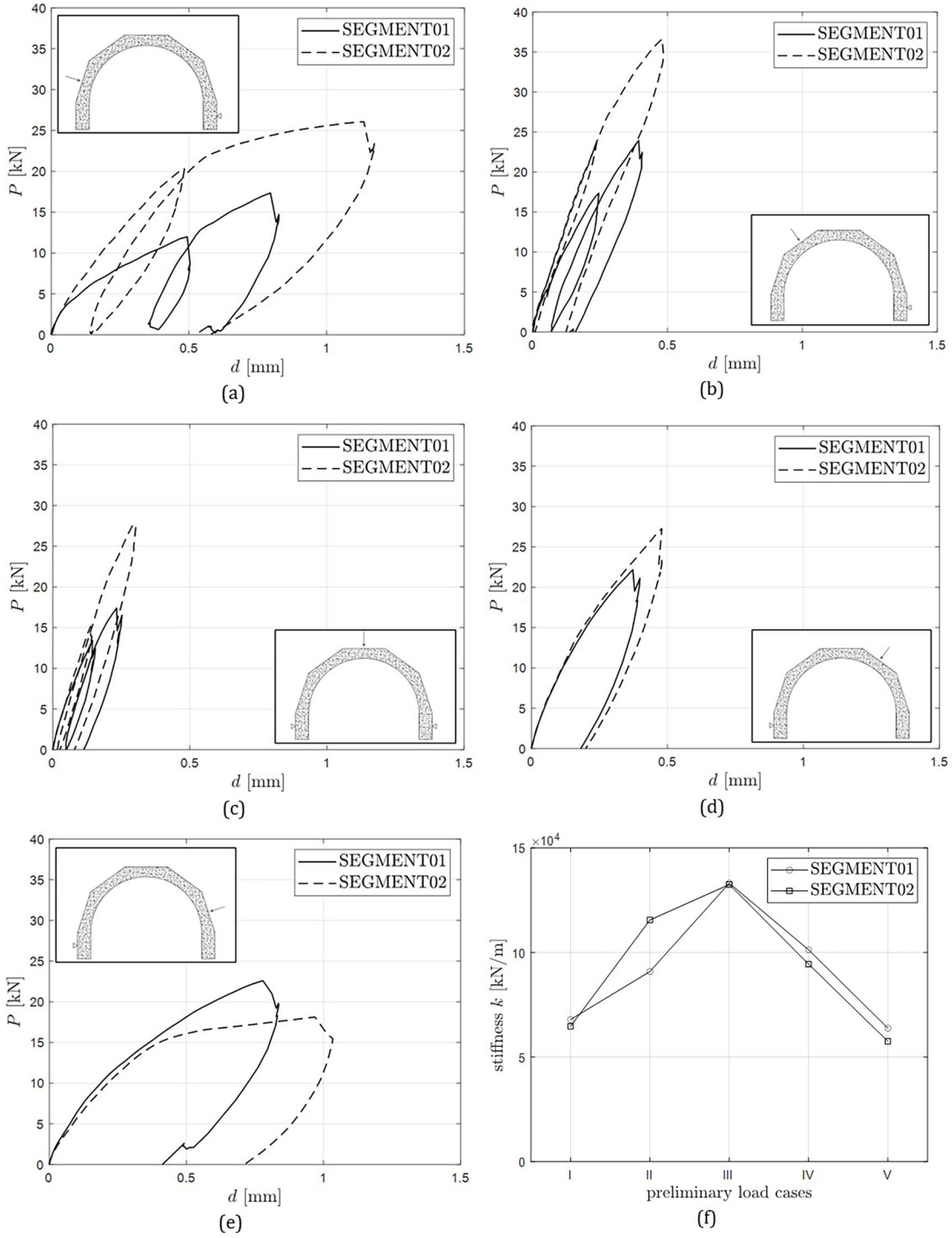


Figure 4. Results of the preliminary tests: (a) load case I; (b) load case II; (c) load case III; (d) load case IV; (e) load case V; (f) comparison on the stiffness values with respect to the different load cases.

Failure loading combinations

Prediction of behaviour

Two different load combinations (LC1 and LC2 reported in Table 1) have been designed to test the mock-ups up to failure. A preliminary numerical analysis was performed in order to evaluate the bending moment distribution, and thus to predict the cross-section of interest for the DIC analysis.

A simple Finite Element model was developed, through the use of 1D Timoshenko beam elements using the commercial software Midas Gen. The geometry of the mock-up has been reproduced using varying cross-section elements, as reported in Figure 5.

Both load combinations were modelled, reproducing the loading and restraining conditions of the mock-ups. As it can be noted in Figure 5a, for LC1 the legs of the specimen are simply supported and actuators 5 and 7 provide a support for the mock-up, whereas actuator 2 is applying a load which is directed on the centre of the mock-up. Similarly for LC2 (Figure 5b), the legs are simply supported and actuators 1 and 7 are restraining the mock-up whereas actuators 3 and 5 are applying the load.

For the preliminary model, a linear elastic analysis was performed using the numerical model. The material properties inputted in the model are thus simply the Young's Modulus (which value of 40 GPa has been computed from Model Code 2010 equation starting from the value of the average compressive strength) and Poisson ratio (assigned of 0.2). The results of interest of the linear elastic analysis are the distributions of the bending moment in the structure for the different loading combinations. Using the obtained bending moment distribution, it is possible to predict the cracking of the mock-up, and thus the placement of the cameras for the DIC analysis. In Figure 6 the bending moment distributions are reported.

According to the results of the preliminary numerical model, it is worth noting that for LC1 the bending moment distribution suggests the formation of cracking of the mock-up in correspondence to actuator 5 which works as restraint, as well as in a position on the left of the key, in between actuators 3 and 4. For the LC2, the bending moment distribution remarks a possible cracking formation in correspondence of actuator 3 and 5, which are loading the mock-up. It is evident that for both the loading combinations a crack may form in correspondence of actuator 5. For this reason, it has been decided that the camera adopted for the DIC analyses the region in correspondence to actuator 5.

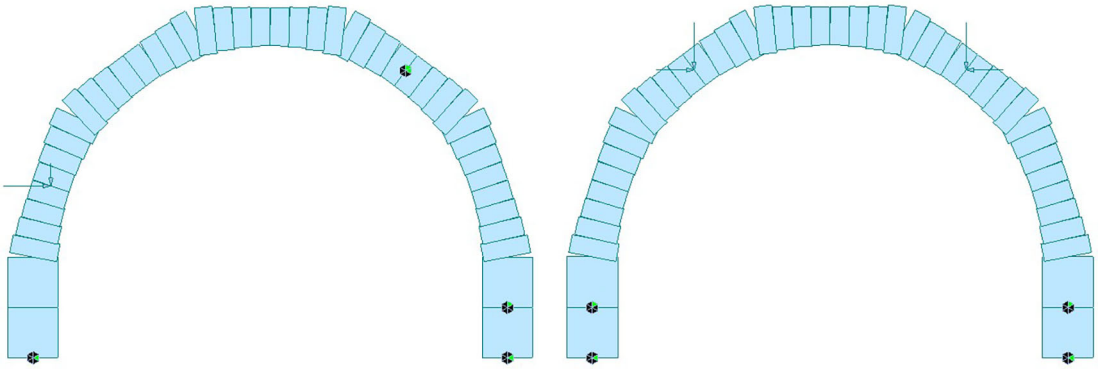


Figure 5. 1D beam model with varying cross-section elements: (a) LC1 and (b) LC2.

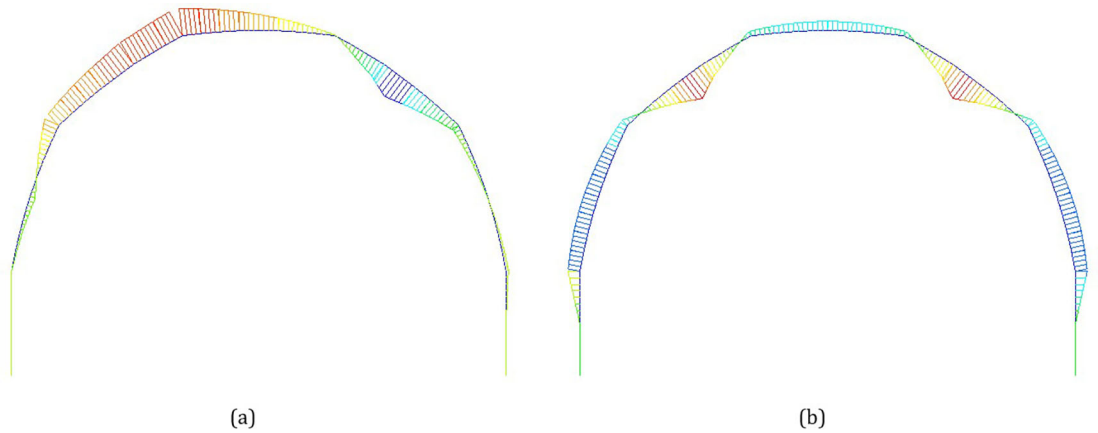


Figure 6. Bending moment distributions for the two different loading combinations: (a) LC1 and (b) LC2.

Collapse of the mock-ups

In this section the collapse of the mock-ups under the two loading combinations will be analysed, starting from the visualisation of the failure mechanism of the specimens and their structural behaviour, up to the study of the cross-sectional behaviour using the DIC analysis.

The failure mechanism of the mock-ups under the different load combinations have been correctly predicted by the bending moment distribution of the preliminary numerical model. In fact, as it can be noted in the collapsed specimen of Figure 7, the cracking formation position coincides with the predicted bending moment distribution. For LC1 two cracks formed after the collapse of the mock-up, one with the opening on the extrados surface and the other with the opening in the intrados surface (as correctly predicted by the sign of the bending moment distribution). For LC2 three cracks formed after the collapse of the specimen, with the first two "positive cracks" predicted by the bending moment distribution, and a third one generated by a negative bending moment at the key. This last crack has not been predicted by the preliminary model which limits its predictions until the elastic limit of the structure. However, due to the inelastic nature of the specimen, as well as the degree of redundancy, additional cracks may form on the mock-up.

With the aim of visualising the structural behaviour of the mock-up for the different load combinations, the load-displacement curves in Figure 8 were obtained.

For both load combinations, the mock-up was able to increase the value of the load after the formation of the cracks. For LC2, due to the larger compressive stresses in the structure, the hardening behaviour is more pronounced, as the ultimate load achieved by the specimen is much higher compared to the one obtained in LC1. In the latter case, the confinement pressure induced by the load combination is almost zero, as the static scheme does not favour the arch effect as for LC2.

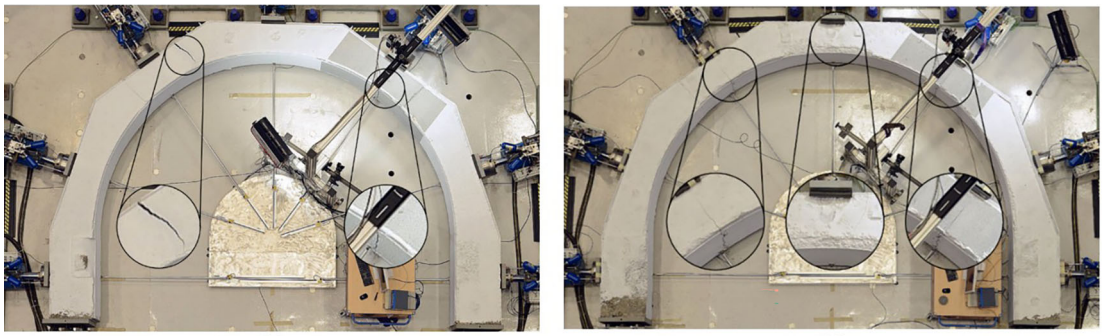


Figure 7. Cracking formation after collapse of the mock-ups: (a) LC1 and (b) LC2.

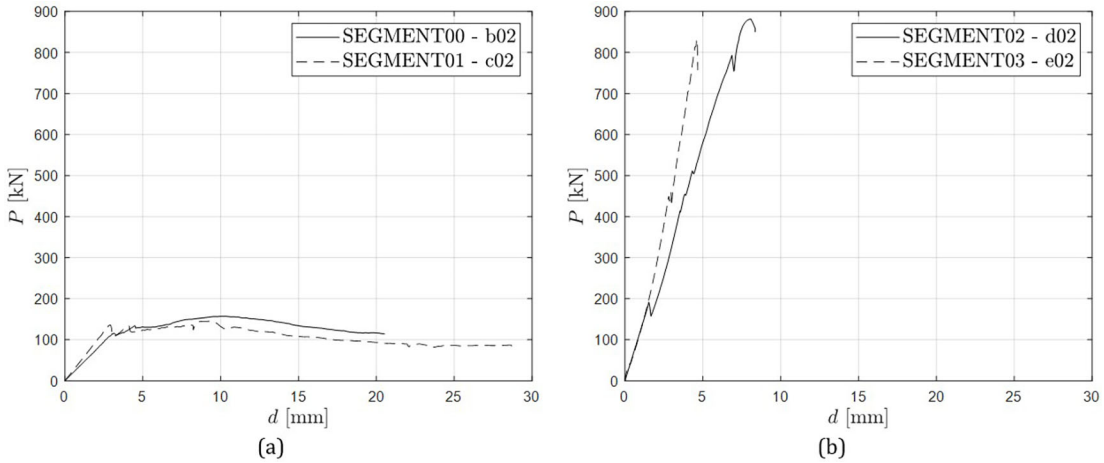


Figure 8. Load versus displacement curves for (a) LC1 and (b) LC2.

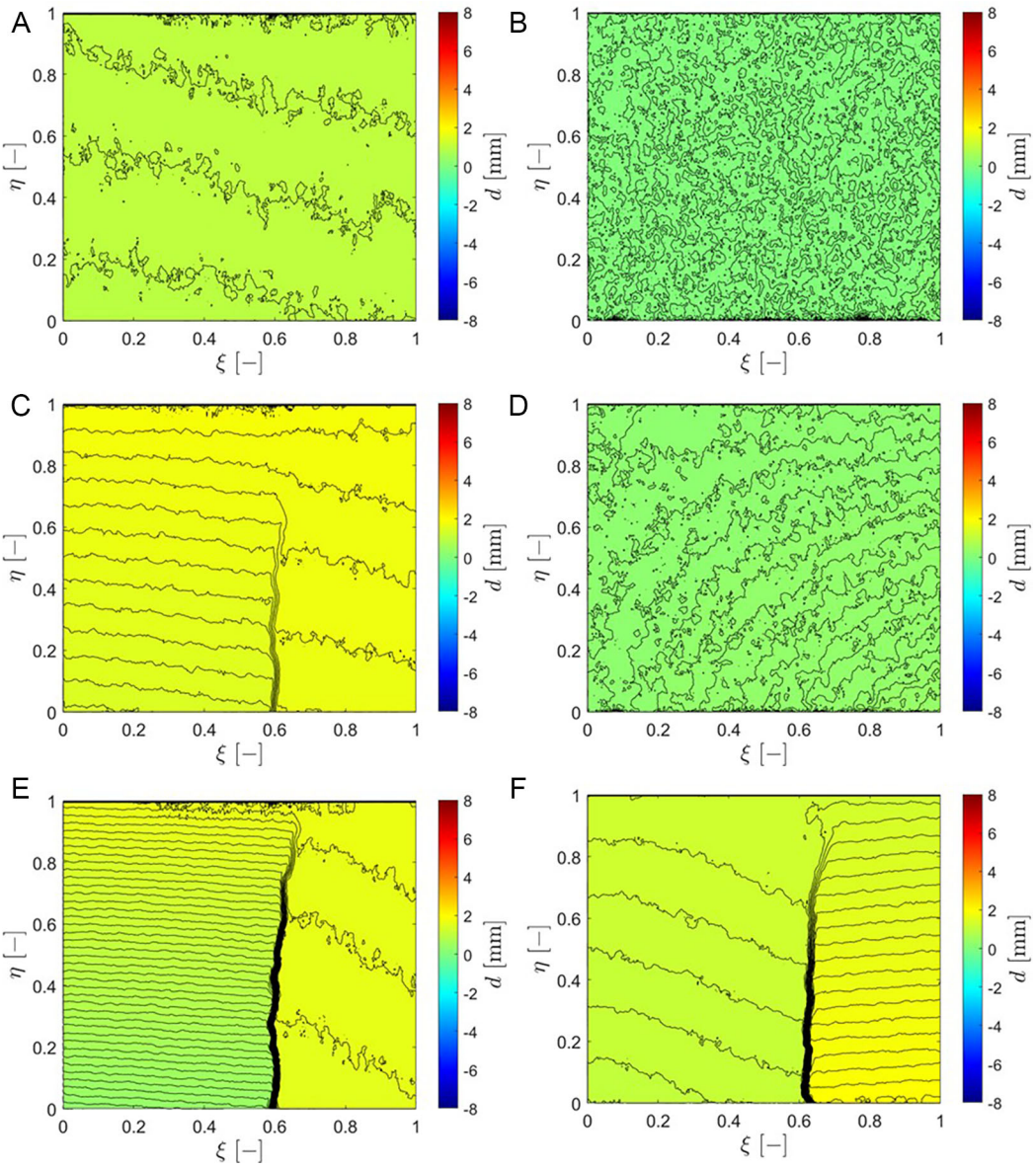


Figure 9. Displacement fields for the different limit states. Figures (A)-(C)-(E)-(G)-(I)-(K) refer to LS1-5 and LScr for Mock-up 2, whereas figures (B)-(D)-(F)-(H)-(J)-(L) for Mock-up 3.

For this reason, in LC1 the post-cracking behaviour of the structure is entirely provided by the fibre reinforcement in the cracked cross-sections.

Digital Image Correlation

As previously discussed, the cross-section analysed using DIC is the one in correspondence to actuator 5, in the proximity of which a speckle pattern has been applied (see Figure 3b). During the tests, the camera acquired images at a frequency of 0.2 Hz, and their analysis was made possible using the "ncorr" plug-in of the commercial software Matlab.[27] The software processes the sequence of frames and studies the variation of speckle position with respect to the reference frame (in terms of pixels) in order to develop the displacement and strain fields for each frame for a specific Region Of Interest (ROI) selected by the user. Finally, the calibration frame ensures conversion from pixels to millimetres. For this specific experimental campaign, only the DIC analyses for mock-up 2 and 3 are available.

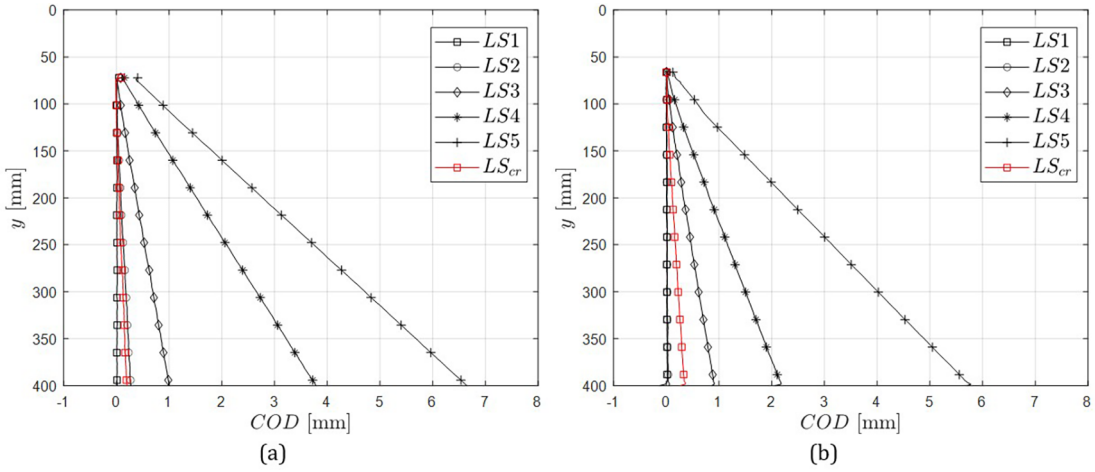


Figure 10. COD profiles along the cross-section height for (a) the mock-up 2 loaded according to LC1, and (b) the mock-up 3 loaded according LC2.

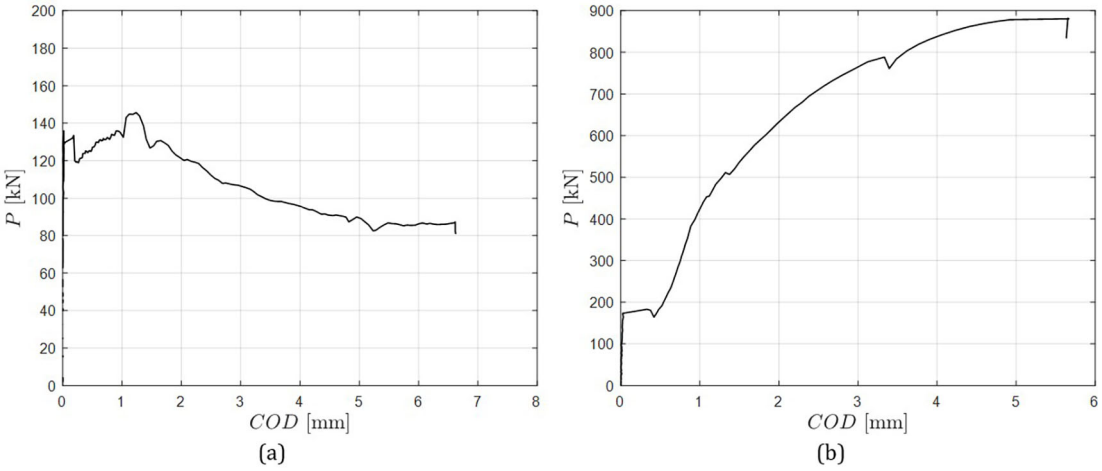


Figure 11. Load versus COD curves for (a) mock-up 2 loaded according to LC1, and (b) mock-up 3 loaded according to LC2.

Through the DIC analysis it is possible to study the displacement field of the region of interest for each frame. From the displacement field it is thus possible to visualise and quantify the crack opening during the test. It is thus meaningful to select specific limit states for the quantification of the crack opening. For example, one may define the limit states with respect to the total displacement computed by the loading actuator. In this case, six limit states have been defined, as percentage of the final displacement: in particular five limit states have been identified corresponding to 20%, 40%, 60%, 80% and 100% of the final displacement (namely LS1, LS2, LS3, LS4 and LS5), and a sixth limit state corresponding to the formation of the crack (identified as LS_{cr}). In Figure 9 the displacement field contour plot are reported, referring to a non-dimensional ROI defined by the ξ and η coordinates, which assume values varying from 0 to 1.

It is worth noting that right after the formation of the crack (LS_{cr}), this generates a localised discontinuity in the displacement field. The higher the limit state, the larger the discontinuity in the displacement field. This can also be quantified as crack opening, by simply considering the difference between the displacements of two points on either side of the crack. In particular, it is possible to compute the variation of the Crack Opening Displacement (COD) along the cross-section for each limit state. Defining the cross-section axis as y, which varies between 0 mm (in correspondence of the extrados) and 400 mm (in correspondence of the intrados), the COD profiles in Figure 10 are obtained.

The COD profiles confirm previous observations, as the crack opening evolves with the limit state. Moreover, it is worth noting that the COD varies linearly along the cross-section for each limit state, meaning that the cracked cross-section rotates remaining flat in its plane.

Through the DIC analysis the COD was computed for each image time step, which was related to the load in the curves shown in Figure 11. Here, the load corresponds to that applied by the loading actuator (actuator 2 for LC1 and actuator 5 for LC2), and the COD corresponding to the one obtained by DIC analysis of the region in proximity of actuator 5 for both load combinations.

It is worth noting that for both mock-ups (thus for both load combinations) the fibre reinforcement enhances the structural performance of the specimens. For LC1 the cracking load registered is close to 140 kN, which is lower than the one obtained for LC2 which reaches a value close to 180 kN. After the formation of the crack, the load increases thanks to the residual tensile strength provided by the fibre bridging mechanism. Due to the fibre presence in the mock-ups, the cracked cross-sections have been able to reach high value of COD (close to 7 mm for LC1 and to 6 mm for LC2), keeping the value of the load high. As already examined, the hardening observed in the mock-up 3 loaded by LC2 is much larger than the hardening obtained for the other mock-up. In fact, for LC1 the maximum load achieved is equal to 145 kN, whereas for LC2 the maximum load is equal to 890 kN. This large difference is provided by the confinement effect generated by LC2, induced by the compressive stress distribution in the mock-up, which increases the load required for the failure of the specimen.

Conclusions

The extrusion-based technology explored in this research project represents a significant advancement for the renovation of existing tunnels, combining increased productivity with superior mechanical performance of the final structure, thanks to a tailored material approach. A key aspect of the validation process, as demonstrated by the experimental program presented in this paper, involves full-scale testing of slip-formed mock-ups under various load combinations, replicating realistic structural service scenarios.

From the preliminary load cases the symmetric behaviour of the mock-up samples has been assessed, remarking the increase of the stiffness value as the load case moves to the key of the tunnel, where the structure is able to exploit the arch effect. The structural tests have highlighted the post-cracking toughness of the mock-ups provided by the fibre reinforcement. The effect of the steel fibres is evident both in terms of load-displacement and load-COD curves. In particular, in the second case, it is worth noting the hardening behaviour of the mock-up for both the symmetric and non-symmetric loading combinations, in which the load increases after the formation of the crack, thanks to the fibre bridging mechanism, which develops in the cracked cross-sections. This underlines how the application of a final lining made of this composite is enough to guarantee the structural safety of the renovated existing tunnel.

Thanks to the toughness improvement in the structural behaviour of the tunnel provided by the steel fibre reinforcement, a partial or even total replacement of the steel reinforcement might be possible for real practice applications, easing the maintenance intervention process and improving its overall productivity.

Ethics and consent

Ethical approval and consent were not required.

Data availability

This paper briefly presented the main results and data generated in the Extruded Tunnel Lining Regeneration Project (ETLR) project. The dataset, gathering quantitative information and metadata, is made available by the authors in line with the requirement of the framework of the Open Access to JRC Research Infrastructures. The complete dataset can be downloaded at https://doi.org/10.5281/zenodo.17396220.[28]

Data are available under the terms of the Creative Commons Attribution 4.0 International.

In order to understand the structure of the shared dataset, the reader should refer to the Technical Report JRC141264.[29]

The main contents of the dataset include: (i) detail of the specimens, (ii) applied loading patterns, (iii) details and calibration reports relative to the installed instrumentations. The calibration of the sensors was performed according to the calibration procedure described in Technical Report No JRC139347.[30] Besides, for each test, the dataset includes: (i) raw data as recorded by the acquisition system of the ELSA lab, (ii) processed data for an easier access to the output of the monitoring, (iii) graphical representation of the main response quantities, (iv) photo sequences taken during the execution of the testing protocol.

Acknowledgements

The first author acknowledges the support of the Italian National Program PON Ricerca e Innovazione in co-funding his PhD scholarship.

References

1. Bilotta E, *et al.*: *Handbook on Tunnels and Underground Works: Volume 1: Concept–Basic Principles of Design.* CRC Press; 2022.
Publisher Full Text

2. Cardu M, Seccatore J: **Quantifying the difficulty of tunneling by drilling and blasting.** *Tunneling and Underground Space Technology.* 2016; **60**: 178–182.
Publisher Full Text

3. Huang L, Bohne RA, Bruland A, *et al.*: **Environmental impact of drill and blast tunnelling: Life cycle assessment.** *J Clean Prod.* Jan. 2015; **86**: 110–117.
Publisher Full Text

4. Maidl B, Herrenknecht M, Maidl U, *et al.*: *Mechanised Shield Tunneling.* Berlin:2nd ed 2012.
Publisher Full Text

5. Salimi A, Rostami J, Moormann C, *et al.*: **Introducing Tree-Based-Regression Models for Prediction of Hard Rock TBM Performance with Consideration of Rock Type.** *Rock Mech Rock Eng.* Aug. 2022; **55**(8): 4869–4891.
Publisher Full Text

6. Xu ZH, Yu TF, Lin P, *et al.*: **Integrated geochemical, mineralogical, and microstructural identification of faults in tunnels and its application to TBM jamming analysis.** *Tunnelling and Underground Space Technology.* Oct. 2022; **128**: 104650.
Publisher Full Text

7. Marcucci A, Vegeto E, Arbelaez JMT, *et al.*: **LIFE CYCLE ASSESSMENT COMPARISON BETWEEN TRADITIONAL AND INNOVATIVE TUNNEL RETROFITTING APPROACHES.** *Spring Convention & conference on advanced construction materials and processes for a carbon neutral society.* Liberato F, Giovanni M, Niki T, editors. Milan: Springer; Apr. 2024.
Publisher Full Text

8. Di Prisco M, Plizzari G, Vandewalle L: **Fibre reinforced concrete: New design perspectives** *Materials and Structures/Materiaux et Constructions.* Nov. 2009; pp. 1261–1281.
Publisher Full Text

9. Wang X, Fan F, Lai J, *et al.*: **Steel fiber reinforced concrete: A review of its material properties and usage in tunnel lining.** *Structures.* 2021; **34**: 1080–1098.
Publisher Full Text

10. Peyvandi AH, Jalali M, Hajsadeghi M, *et al.*: **Experimental investigation on the performance of engineered spiral fiber: Fiber pull-out and direct tension tests.** *Constr Build Mater.* 2022; **347**: 128569.
Publisher Full Text

11. Singh S, Shukla A, Brown R: **Pullout behavior of polypropylene fibers from cementitious matrix.** *Cem Concr Res.* Oct. 2004; **34**(10): 1919–1925.
Publisher Full Text

12. Lo Monte F, Ferrara L: **Tensile behaviour identification in Ultra-High Performance Fibre Reinforced Cementitious Composites: indirect tension tests and back analysis of flexural test results.** *Materials and Structures/Materiaux et Constructions.* Dec. 2020; **53**(6).
Publisher Full Text

13. Valentim DB, Aalet S, Kreger M: **Evaluation of Test Methods to Characterize Tensile Strength of Ultra-High-Performance Concrete.** *ACI Mater J.* Jul. 2022; **119**(4): 165–176.
Publisher Full Text

14. Model code 2010: final draft: **International Federation for Structural Concrete (fib).** 2012.

15. Di Prisco M, Colombo M, Dozio D: **Fibre-reinforced concrete in fib Model Code 2010: Principles, models and test validation.** *Structural Concrete.* 2013; **14**(4): 342–361.
Publisher Full Text

16. Dupont D, Vandewalle L: **Distribution of steel fibres in rectangular sections.** *Cem Concr Compos.* Mar. 2005; **27**(3): 391–398.
Publisher Full Text

17. Ferrara L, Ozyurt N, Di Prisco M: **High mechanical performance of fibre reinforced cementitious composites: The role of 'casting-flow induced' fibre orientation.** *Materials and Structures/Materiaux et Constructions.* Jan. 2011; **44**(1): 109–128.
Publisher Full Text

18. Zerbino R, Tobes JM, Bossio ME, *et al.*: **On the orientation of fibres in structural members fabricated with self compacting fibre reinforced concrete.** *Cem Concr Compos.* Feb. 2012; **34**(2): 191–200.
Publisher Full Text

19. Martinie L, Roussel N: **Simple tools for fiber orientation prediction in industrial practice.** *Cem Concr Res.* 2011; **41**: 993–1000.
Publisher Full Text

20. Huang H, Su A, Gao X, *et al.*: **Influence of formwork wall effect on fiber orientation ofUHPV with two casting methods.** *Constr Build Mater.* 2019; **215**: 310–320.
Publisher Full Text

21. Kolarik F, Patzak B, Thrane LN: **Modeling of fiber orientation in viscous fluid flow with application to self-compacting concrete.** *Comput Struct.* 2015; **154**: 91–100.
Publisher Full Text

22. Seta B, *et al.*: **Numerical modeling of fiber orientation in multi-layer, material-extrusion big area additive manufacturing.** *Addit Manuf.* 2024.
Reference Source

23. Zhao Y, Bi J, Wang Z, *et al.*: **Numerical simulation of the casting process of steel fiber reinforced self-compacting concrete: Influence of material and casting parameters on fiber orientation and distribution.** *Constr Build Mater.* 2021; **312**: 125337.
Publisher Full Text

24. Ferrara L, Faifer M, Toscani S: **A magnetic method for non destructive monitoring of fiber dispersion and orientation in steel fiber reinforced cementitious composites-part 1: Method calibration.** *Materials and Structures/Materiaux et Constructions.* Apr. 2012; **45**(4): 575–589.
Publisher Full Text

25. Ferrara L, Faifer M, Muhaxheri M, *et al.*: **A magnetic method for non destructive monitoring of fiber dispersion and orientation in steel fiber reinforced cementitious composites. Part 2: Correlation to tensile fracture toughness.** *Materials and Structures/Materiaux et Constructions.* Apr. 2012; **45**(4): 591–598.
Publisher Full Text

26. CEN members, EN 14651:2005: **Test method for metallic fibered concrete - Measuring the flexural tensile strength (limit of proportionality (LOP), residual).** 2005.

27. Blaber J, Adair B, Antoniou A: **Ncorr: Open-Source 2D Digital Image Correlation Matlab Software.** *Exp Mech.* Jul. 2015; **55**(6): 1105–1122.
Publisher Full Text

28. Joint Research CentreHinfra P, di Milano MA, *et al.*: ETLR - Extruded Tunnel Lining Regeneration. [Data set]. *Zenodo.* 2025. w
Publisher Full Text

29. Peloso S, Molina FJ, Lamperti Tornaghi M, *et al.*: *ELSA - Structure of the experimental datasets.* Luxembourg: Publications Office of the European Union; 2025. JRC141264.
Publisher Full Text

30. Peloso S, Molina FJ, Lamperti Tornaghi M, *et al.*: *ELSA - Procedure for calibration and verification of displacement and rotation measuring systems.* Luxembourg: Publications Office of the European Union; 2024. JRC139347.
Publisher Full Text